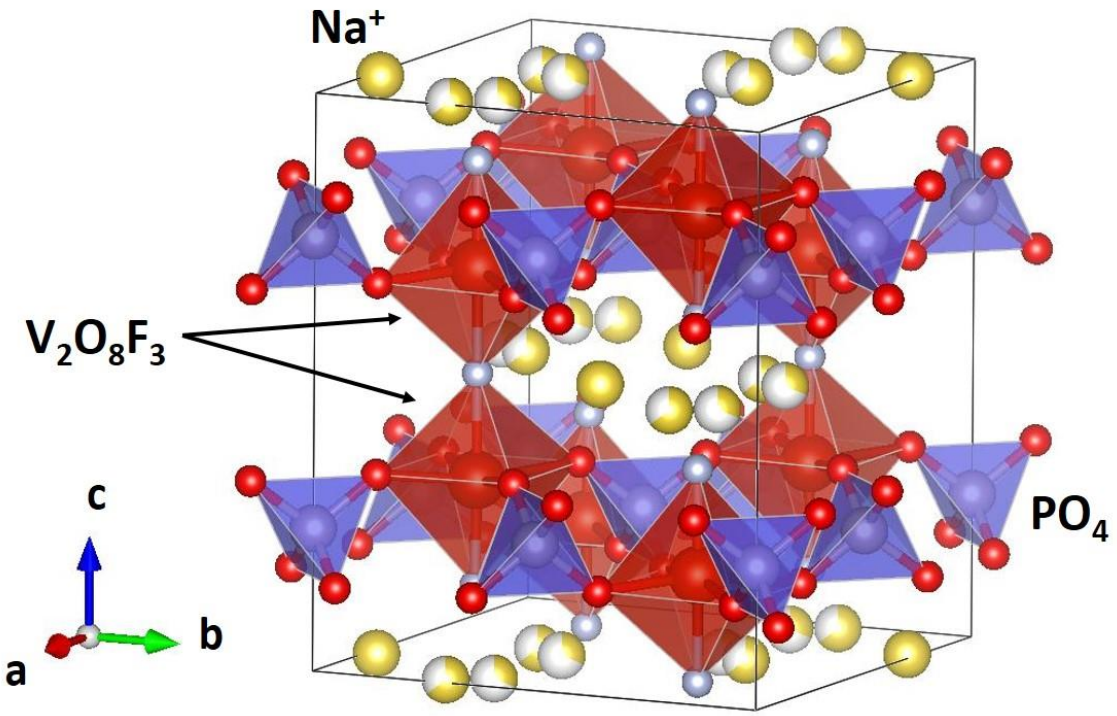

Figure 1 : The 3D crystal structure of $Na_3V_2(PO_4)_2F_3$. The bi-octahedral units $V_2O_8F_3$ and the tetrahedral PO_4 groups are shown as red and violet polyhedra, respectively. The Na^+ ions, represented by yellow balls, occupy the empty space in the structure at the crystallographic planes z = 0 and z = ½.

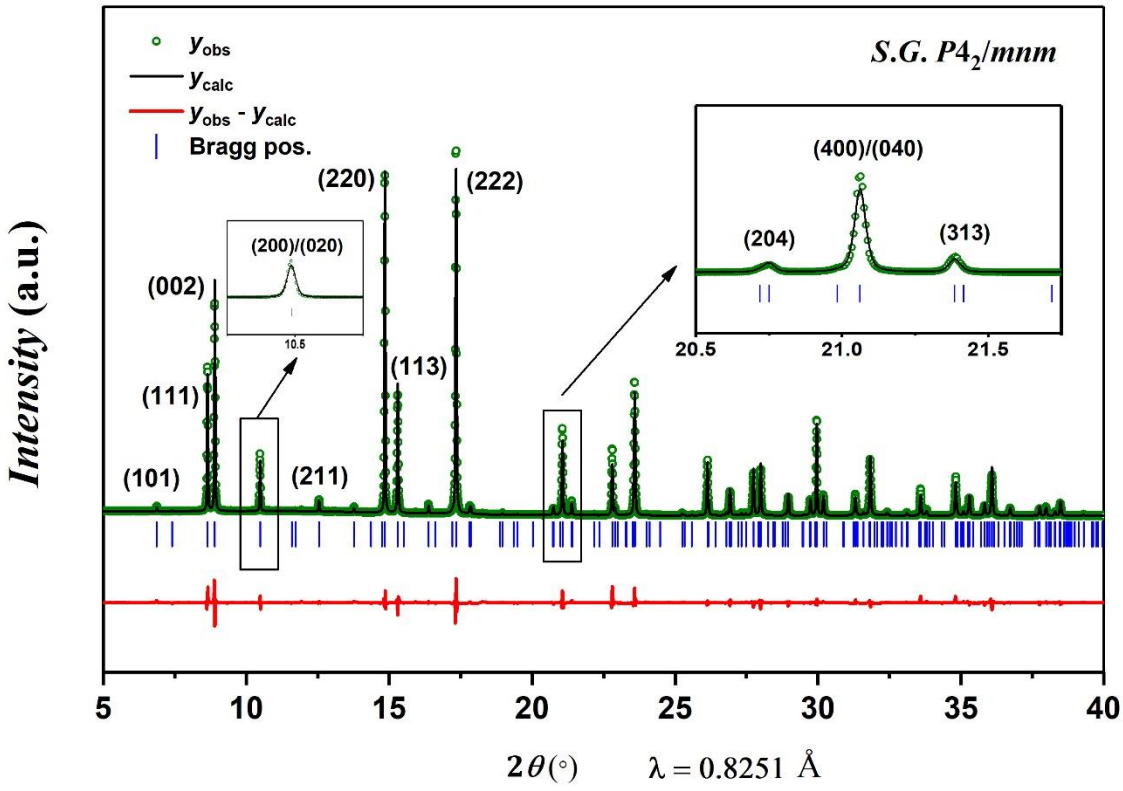

Figure 2 : Rietveld refinement of the $Na_3(VO)Fe(PO_4)_2F_2$ structure from SXRD data, performed in the $P4_2/mnm$ space group. Insets show enlargements of the (200)/(020) and (400)/(040) doublets.

Table 1 : Structural parameters of $Na_3(VO)Fe(PO_4)_2F_2$ obtained from Rietveld refinement of synchrotron powder diffraction data collected at λ = 0.8251 Å. The Biso values of oxygen and fluorine were fixed during the Rietveld refinement.

S.G. P4_2*/mnm*		*a* = *b* = 9.03564(6) Å				R_{Bragg} = 3.46%
Z = 4		*c* = 10.6412(1) Å				R_p = 10.3%
		V/Z = 217.195(2) Å^3				R_{wp} = 10.7%
Atoms	**Wyckoff positions**	***x/a***	***y/b***	***z/c***	**Occupancy**	**B_{iso}**
V(1)	8j	0.7483(6)	0.2517(6)	0.1917(2)	½	0.96(6)
Fe(1)	8j	0.7483(6)	0.2517(6)	0.1917(2)	½	0.96(6)
P(1)	4e	½	½	0.253(2)	1	0.9(1)
P(2)	4d	½	0	¼	1	0.8(1)
O(1)	16k	0.595(2)	0.094(2)	0.162(1)	1	0.78
O(2)	8j	0.598(2)	0.402(2)	0.160(2)	1	0.78
O(3)	8j	0.402(2)	0.402(2)	0.330(2)	1	0.78
O(4)	8j	¾	¼	0.360(2)	½	1.0
F(1)	4g	¾	¼	0	1	0.44
F(2)	8j	¾	¼	0.360(2)	½	1.0
Na(1)	8i	0.270(2)	0.022(2)	0	0.850(3)	2.1(1)
Na(2)	8i	0.476(3)	0.290(3)	0	0.58(1)	4.5(4)
Na(3)	4f	0.408(5)	0.408(5)	0	0.266(6)	3.0(3)

Table 2 : Bond lengths (Å) describing the coordination polyhedra of each cation in $Na_3(VO)Fe(PO_4)_2F_2$ determined from Rietveld refinement performed in the $P4_2/mnm$ space group of synchrotron X-ray powder diffraction data collected at $\lambda = 0.8251$ Å.

	V/Fe	P(1)	P(2)	Na(1)	Na(2)	Na(3)
Coordination	6	4	4	7	7	6
O(1)	1.954(6)	1.595(8)x2		2.619(9)x2	2.27(1)x2	2.42(1)x4
O(2)	2.013(6)		1.529(6) x4		2.70(1)x2	
O(3)	1.983(6)x2	1.493(8)x2		2.351(7)x2		
F(1)	2.040(1)			2.464(7)	2.50(1)	
F(2)/O(4)	1.795(1)			2.547(6)x2	2.55(1)x2	2.50(1)x2

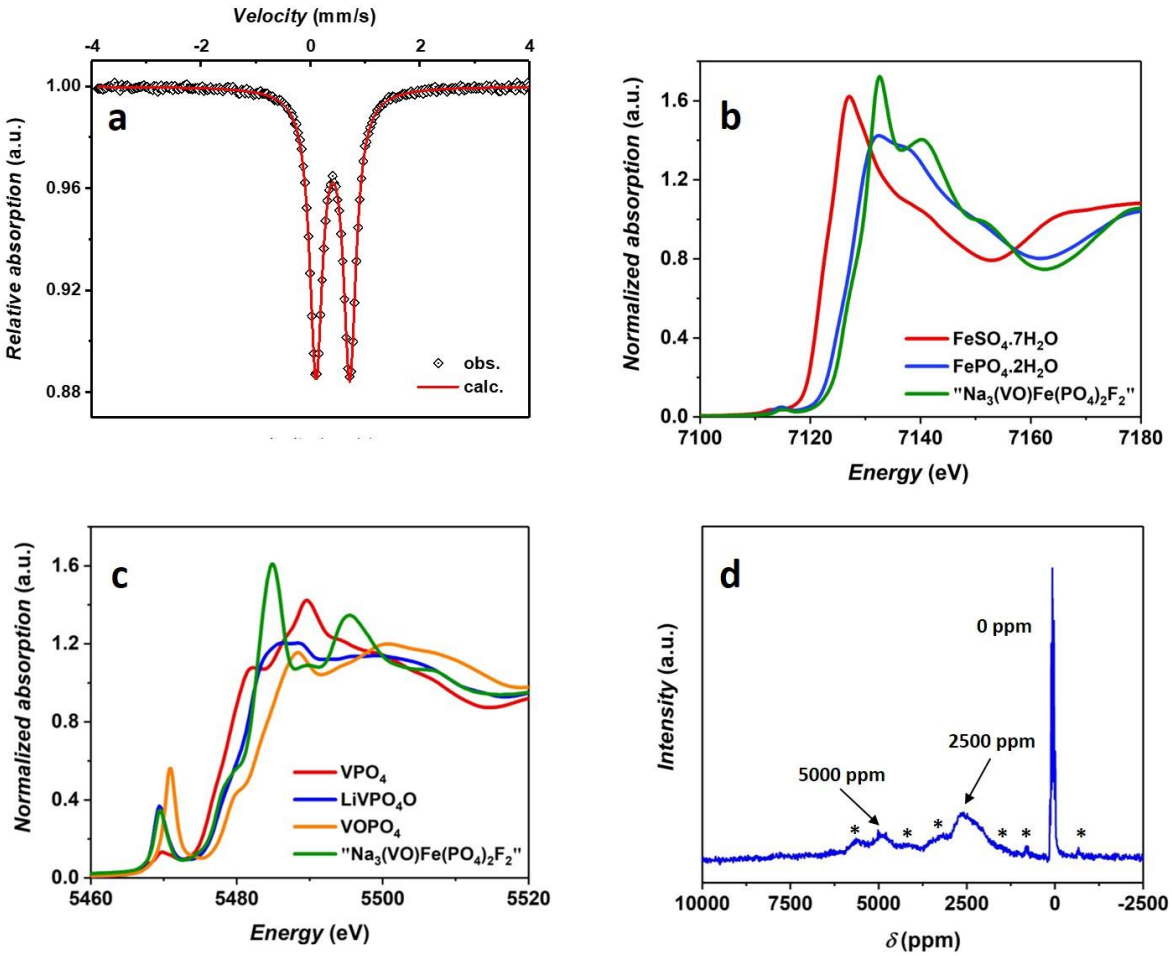

Figure 3 : (*a*) ^{57}Fe Mössbauer spectrum recorded at ambient temperature with a ^{57}Co source, (*b*) Fe K-edge XANES spectrum of $Na_3(VO)Fe(PO_4)_2F_2$. Both $Fe^{2+}SO_4.7H_2O$ and $Fe^{3+}PO_4.2H_2O$ are used as references to determine the Fe oxidation state, (*c*) V K-edge XANES spectrum of $Na_3(VO)Fe(PO_4)_2F_2$. The $V^{3+}PO_4$, $LiV^{4+}PO_4O$ and $V^{5+}OPO_4$ XANES spectra are reported to determine the V oxidation state, (*d*) ^{31}P *ss*-NMR spectrum recorded at 100 MHz, MAS frequency = 30 kHz. The excitation pulse was placed at 5000 ppm. The asterisks (*) indicate the rotational spinning sidebands.

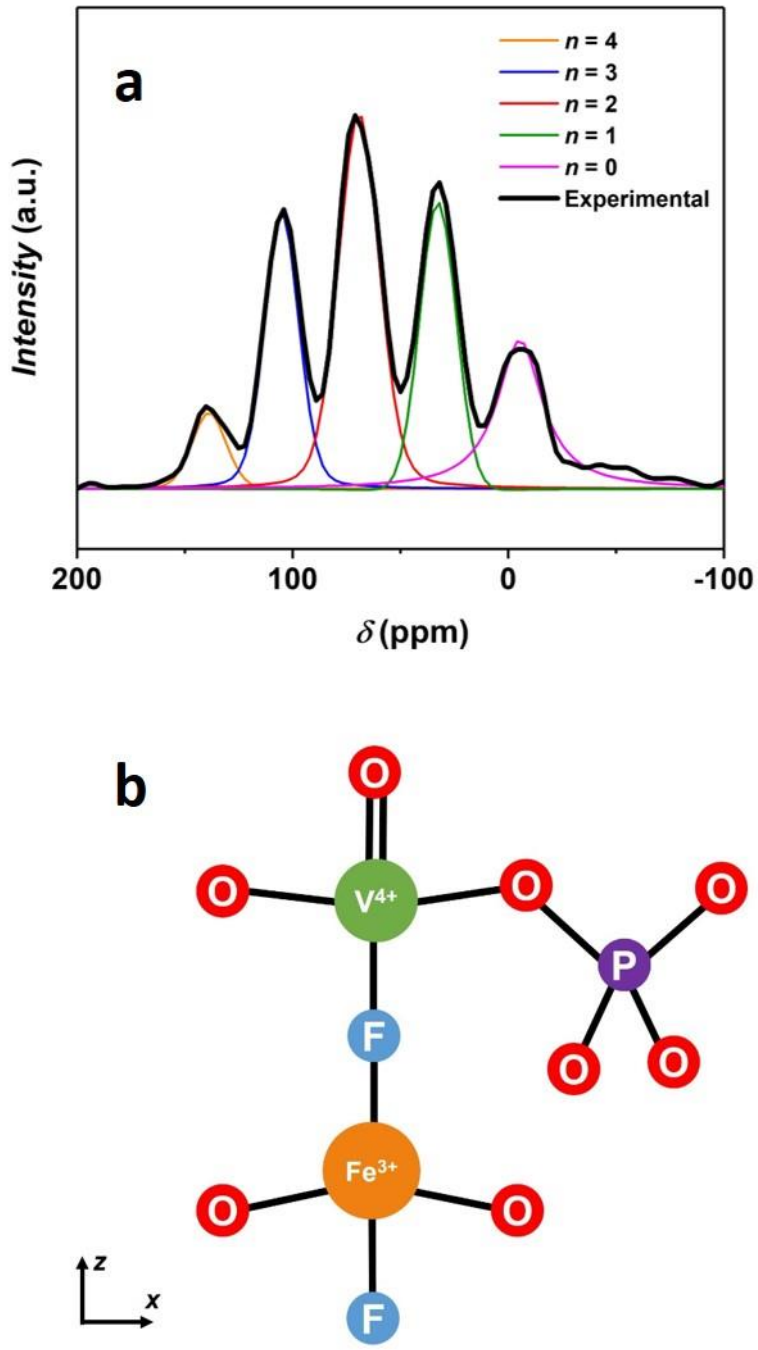

Figure 4 *:* (*a*) An enlargement of the ^{31}P NMR diamagnetic resonances (-100 ppm to 200 ppm) recorded for the $Na_3(VO)Fe(PO_4)_2F_2$ material. The *n* value indicates the number of Fe^{3+} in the second transition metal sites with respect to the Phosphorus nucleus. The five diamagnetic resonances observed for this material can be fitted by five different Pseudo-Voigt peak shape functions, (*b*) Illustration of the influence of the second neighboring metal ion belonging to the bi-octahedral unit on the ^{31}P chemical shift value.

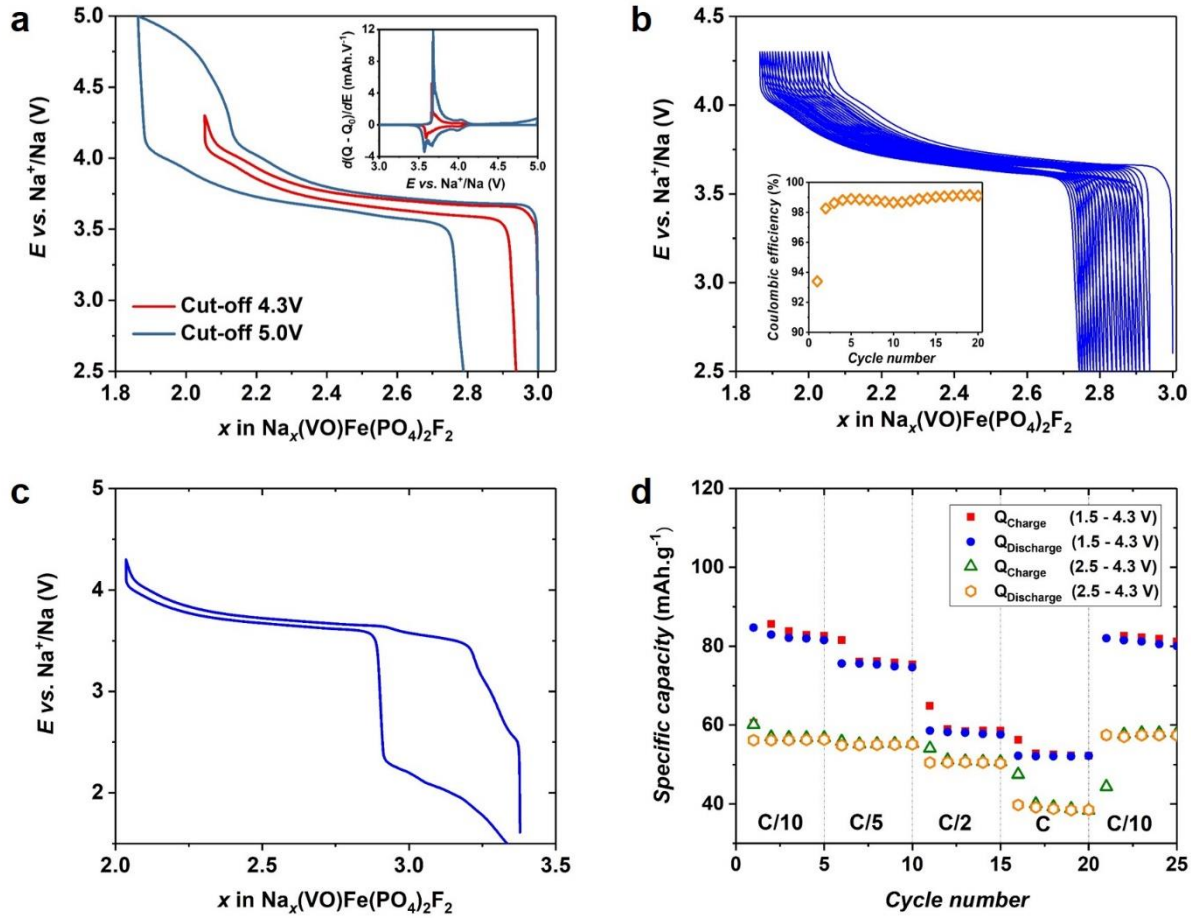

Figure 5 : (*a*) The charge/discharge curve of $Na_3(VO)Fe(PO_4)_2F_2$ vs. Na metal, at *C*/10 cycling rate with the cut-off voltage of 4.3 and 5.0 V vs. Na^+/Na. Inset shows the first derivative charge/discharge curve as a function of the operating voltage, (*b*) The long-term evolution of the charge/discharge curves at *C*/10 cycling rate in the potential range of 2.5 - 4.3 V vs. Na^+/Na. Inset shows the evolution of the coulombic efficiency during the first twenty cycles, (*c*) The charge/discharge curve obtained at the second cycle for $Na_3(VO)Fe(PO_4)_2F_2$ vs. Na metal, at the cycling rate of *C*/10 per Na^+ and in the potential range of 1.5 - 4.3 V vs. Na^+/Na, (*d*) The charge/discharge capacity of $Na_3(VO)Fe(PO_4)_2F_2$ at different cycle rates in the potential ranges of 2.5 - 4.3 V and 1.5 - 4.3 V vs. Na^+/Na.

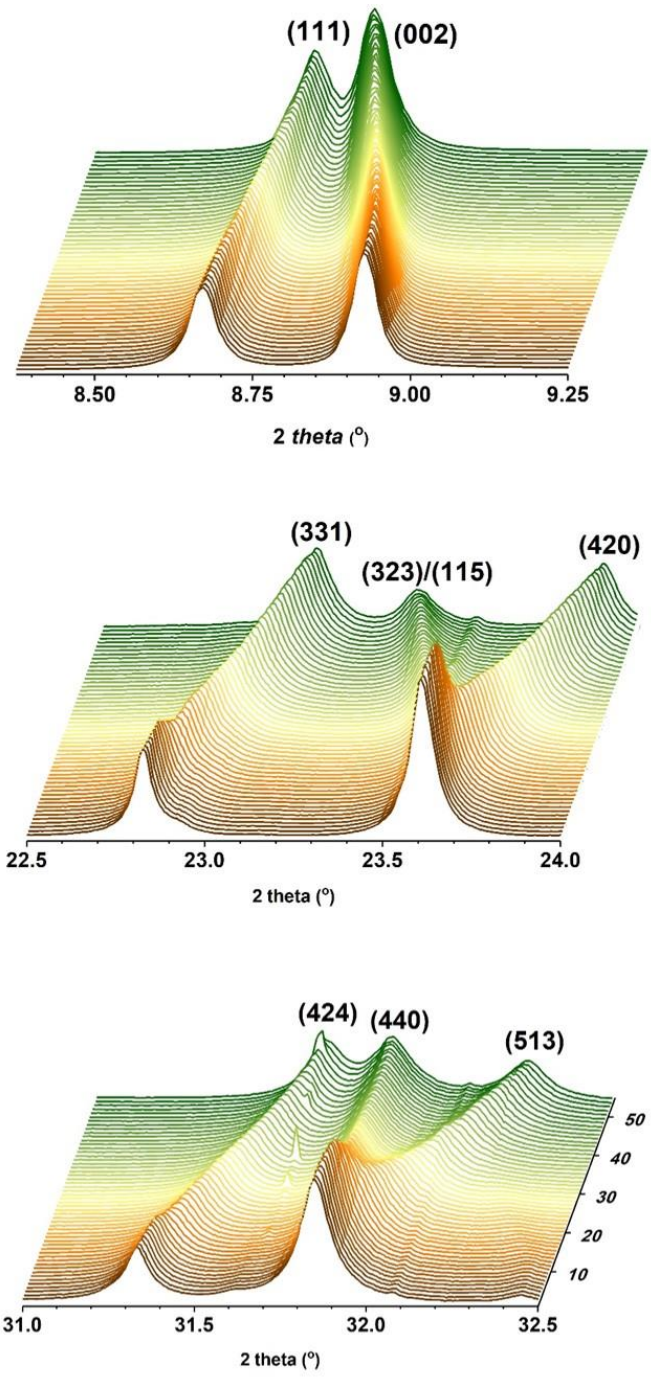

Figure 6 : The evolution of significant diffraction lines during Na^+ de-intercalation from $Na_3(VO)Fe(PO_4)_2F_2$. *Operando* SXRD patterns were recorded upon cycling of a Na// $Na_3(VO)Fe(PO_4)_2F_2$ half-cell at λ = 0.8251 Å. The cell was cycled at C/10 cycling rate in the voltage window of 2.5 - 4.3 V vs. Na^+/Na. The corresponding electrochemical data is given in **Figure S12**.

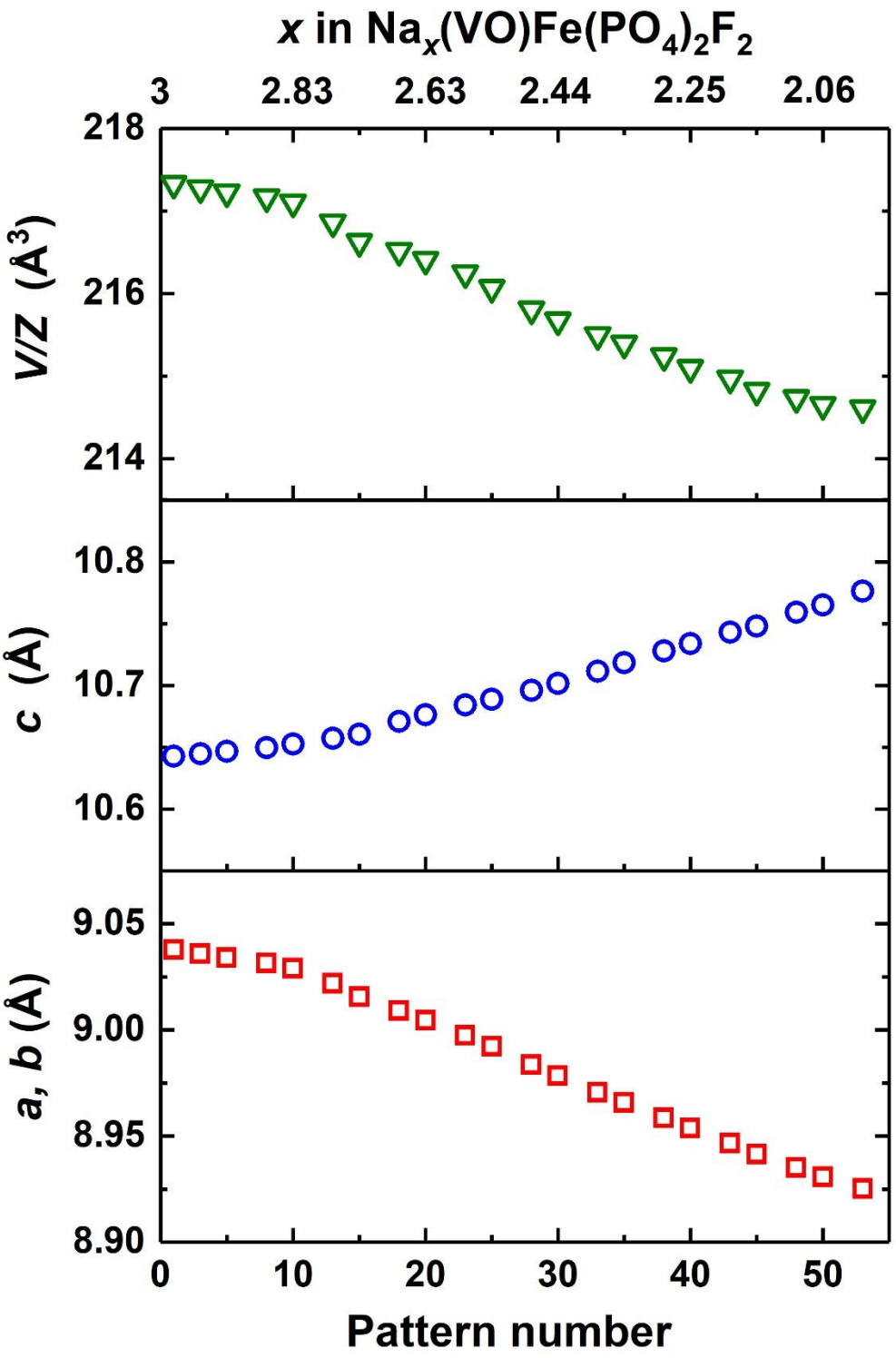

Figure 7 : The evolution of the cell parameters of $Na_{3-x}(VO)Fe(PO_4)_2F_2$ during the Na^+ de-intercalation reaction, determined from the Le Bail fit of the SXRD patterns collected *operando* upon charging a $Na//Na_3(VO)Fe(PO_4)_2F_2$ half-cell.

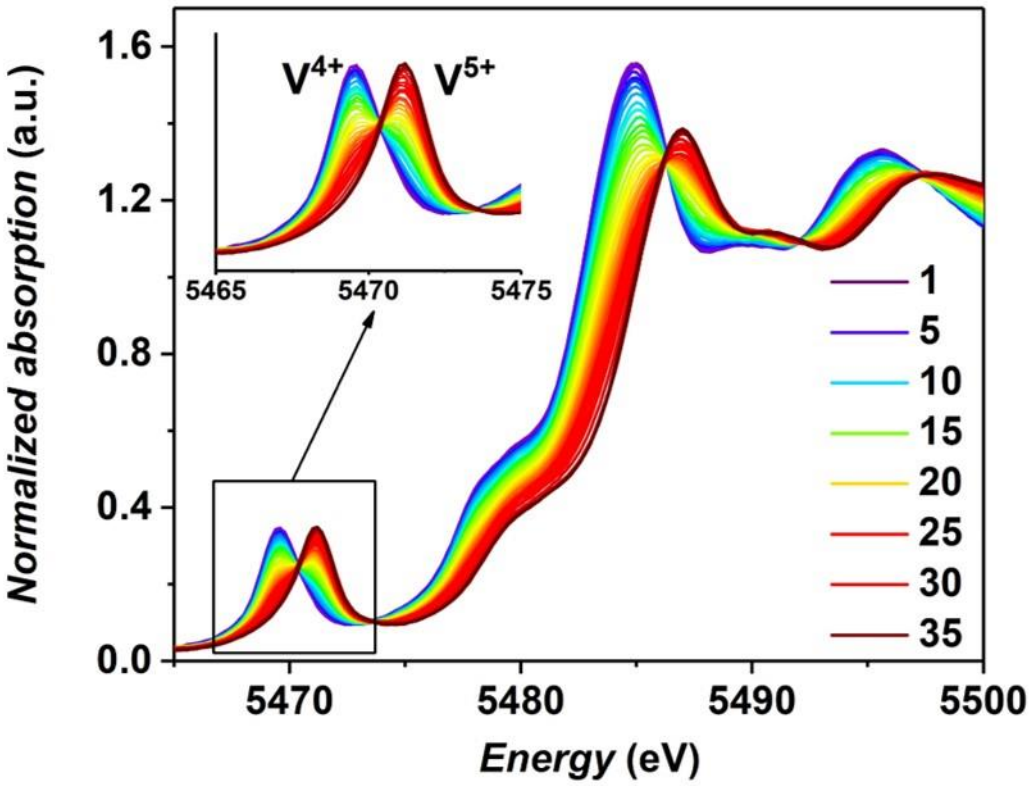

Figure 8 : Vanadium K-edge XANES spectra recorded *operando* upon charging a Na//$Na_3(VO)Fe(PO_4)_2F_2$ half-cell operating in the potential range of 2.5 - 4.5 V vs. Na^+/Na (**Figure S14**).

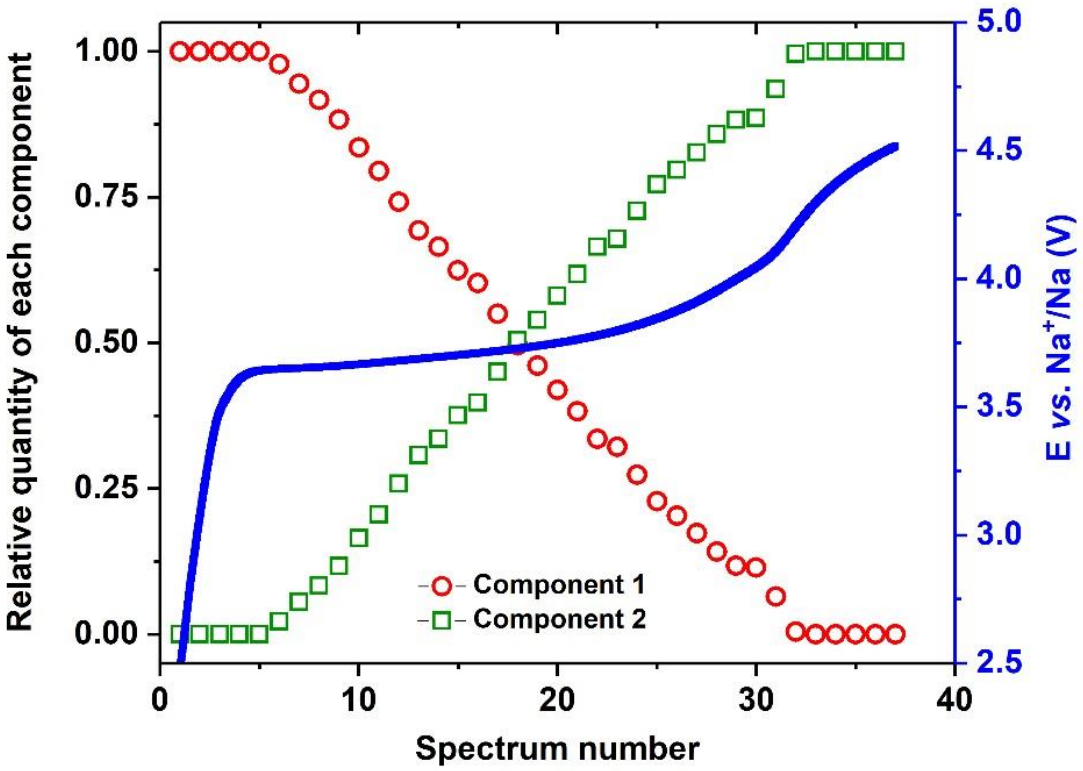

Figure 9 : The evolution of the concentration of the two principal components required to describe all the Vanadium K-edge XAS spectra recorded upon charging a Na//$Na_3(VO)Fe(PO_4)_2F_2$ half-cell. The cell was cycled at *C*/10 in the voltage window of 2.5 - 4.5 V vs. Na^+/Na.